CHEMISTRY OF MATERIALS

Article

pubs.acs.org/cm

Stable and Multifunctional Dye-Modified Black Phosphorus Nanosheets for Near-Infrared Imaging-Guided Photothermal Therapy

Yuetao Zhao,[†] Liping Tong,[†] Zhibin Li,[‡] Na Yang,[†] Haidi Fu,[†] Lie Wu,[†] Haodong Cui,[†] Wenhua Zhou,[†] Jiahong Wang,[†] Huaiyu Wang,[†] Paul K. Chu,[‡] and Xue-Feng Yu*[,†]

[†]Institute of Biomedicine and Biotechnology, Shenzhen Institutes of Advanced Technology, Chinese Academy of Sciences, Shenzhen 518055, P. R. China

[‡]Department of Physics and Materials Science, City University of Hong Kong, Tat Chee Avenue, Kowloon, Hong Kong, China

Supporting Information

ABSTRACT: Nanomedicines intergrating both therapy and diagnosis functions provide a promising strategy for anticancer treatment. As novel two-dimensional materials, black phosphorus nanosheets (BPs) possess unique properties for biomedical applications, pratically for photothermal therapy (PTT) of cancer, but their lack of air and water stability may hinder their application. Herein, a covalent functionalization strategy based on Nile Blue (NB) dye via diazonium chemistry is established to modify BPs, not only enhancing the stability of BPs but also rendering BPs via near-infrared (NIR) fluorescence, forming a novel multifunctional nanomedicine with both PTT and NIR imaging capabilities. *In vitro* tests demonstrate that the dye-modified BPs (named NB@BPs) have good biocompatibility and exhibit strong PTT and NIR imaging efficiency. *In vivo* experiments show that the NB@BPs can mark the tumor site with red fluorescence and lead to efficient tumor ablation under NIR irradiation. These results reveal a potential BP-based nanomedicine with multiple functionalities that bode well for anticancer applications.

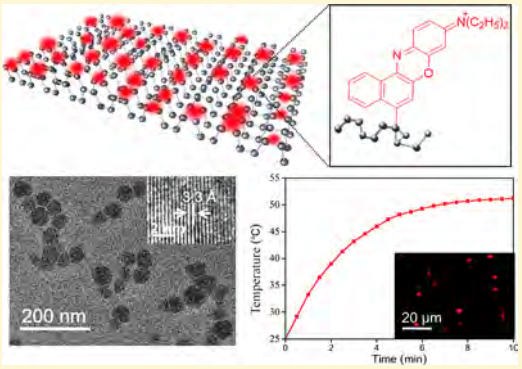

INTRODUCTION

Nanomaterials that interact with near-infrared (NIR) light provide a unique opportunity in biophotonic nanomedicine.[1] On the basis of the light-activatable multimodal nanoparticles, imaging-guided therapy can be designed. A typical example is the integration of strong NIR absorption and fluorescence capabilities into a single nanostructure enabling imaging-guided photothermal therapy (PTT) for cancer.[2,3] To date, different kinds of nanoparticles have been proposed as optical nanomedicines for bioimaging and/or therapy, such as metallic nanostructures, metal-based semiconductor nanoparticles, carbon nanomaterials, etc.[4−17] However, even with promising application potential, most of them still suffer from poor biodegradability, and concerns about deleterious effect remain.[18] Hence, developing new strategies for producing biodegradable multifunctional nanomaterials with capacity for synergistic combination therapy is still the main challenge.

As a new member of the family of two-dimensional (2D) materials, black phosphorus (BP) has received much interest because of its unique 2D layered structure and layer-dependent bandgap of 0.3−2.0 eV.[19] Atomically thin BP nanosheets (BPs) with different lateral sizes can be synthesized by using different strategies such as liquid exfoliation.[20−25] Because of its excellent optical properties such as strong NIR absorption and high photothermal conversion efficiency, BPs have recently been adopted medically for photothermal therapy,[26] photodynamic therapy,[27] and drug delivery.[28] Compared to other nanoparticles, BP can degrade in aqueous media forming nontoxic phosphate and phosphonate.[29−31] Furthermore, phosphorus is one of the essential elements in human organs, making up ∼1% of the total body weight,[32−34] and is inherently biocompatible. However, atomically thin BPs are very reactive in the presence of oxygen and water, thus causing rapid degradation of the optical performance in aqueous media.[35−38] This problem has hitherto hampered in-depth investigation and application of BPs to biophotonic nanomedicine.

The degradation mechanism of BPs has recently been clarified, and much effort has been devoted to prevent the rapid degradation of BPs via chemical modification.[39−43] For instance, we have proposed a surface coordination strategy in which titanium sulfonate ligand coordination enhances the stability of BPs in air and water.[39] A covalent modification scheme utilizing diazonium salts has been proposed by Hersam and co-workers[41] to enhance the air stability of BPs in nanoelectronic applications, and a perylene-3,4,9,10-tetracarboxylic dianhydride (PTCDA) molecule self-assembly method

Received: March 17, 2017
Revised: June 10, 2017
Published: August 3, 2017

DOI: 10.1021/acs.chemmater.7b01106
Chem. Mater. 2017, 29, 7131−7139

Scheme 1. Synthesis of NB-D from NB

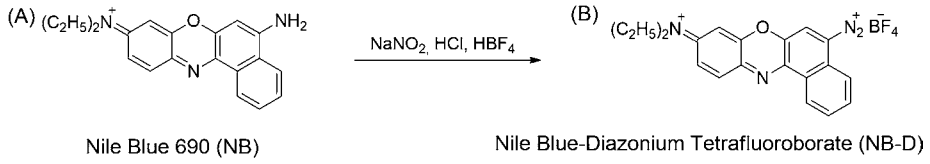

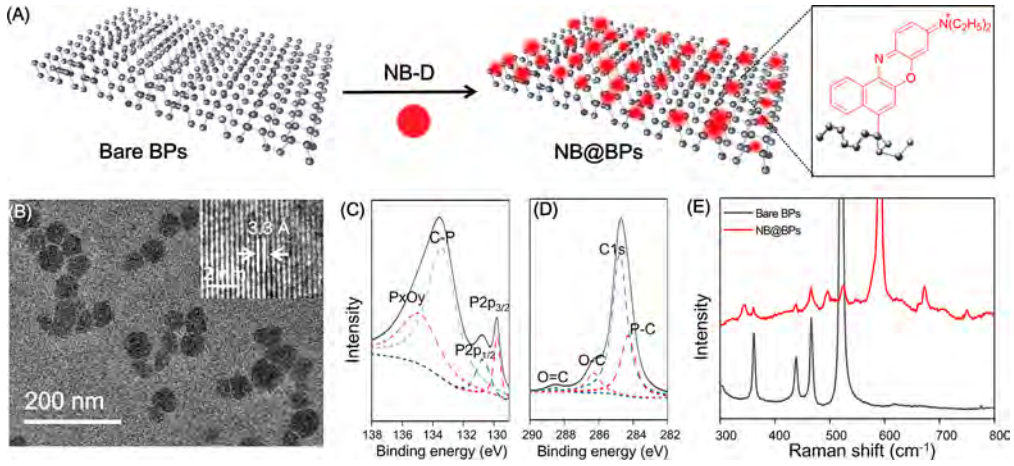

Figure 1. Fabrication and characterization of NB@BPs. (A) Schematic illustration of fabrication of NB@BPs. (B) TEM and inset HR-TEM images. (C) HR-XPS P 2p spectra. (D) HR-XPS C 1s spectra. (E) Raman spectra.

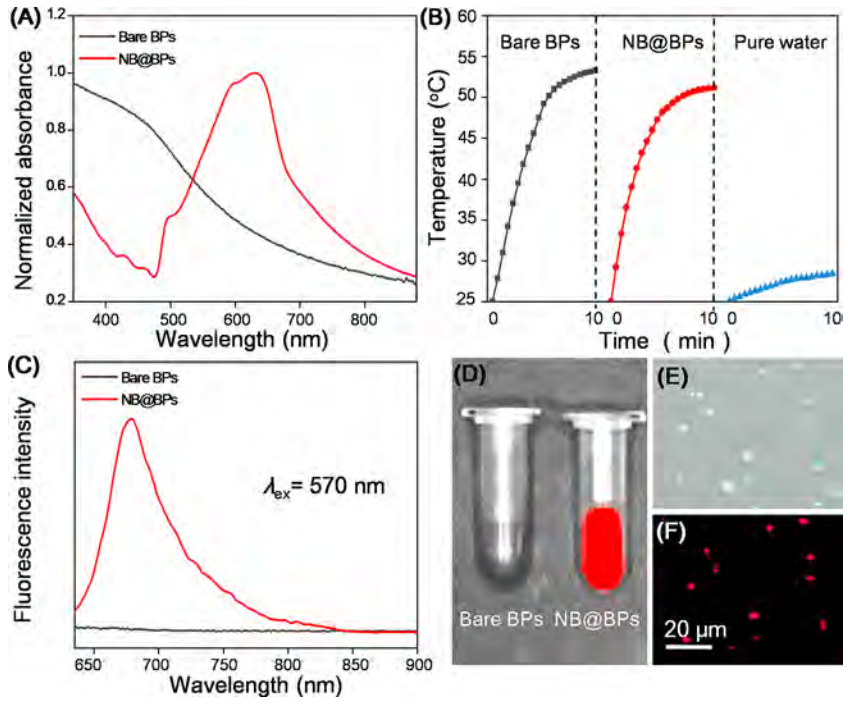

Figure 2. Optical properties of bare BPs and NB@BPs. (A) Absorption spectra. (B) Photothermal heating curves under 808 nm and 1.0 W cm^{-2} laser irradiation. (C) Fluorescence emission spectra (λ_{ex} = 570 nm). (D) Macroscopic fluorescence images (λ_{ex} = 570 nm). (E) Bright-field and (F) fluorescence micrographs of microsized NB@BPs.

has been proposed by Wang and co-workers.[43] In spite of the progress, simple and effective modification strategies are still needed to promote biophotonic application of BPs.

Herein, a modification strategy utilizing a fluorescent dye via diazonium chemistry is described. The fluorescent dye Nile Blue 690 [NB (Scheme 1A)] is converted into its diazonium tetrafluoroborate salt [named NB-D (Scheme 1B)]. NB-D then reacts with BPs, forming stable C−P bonds on the BP surface by aryl diazonium coupling. The NB-modified BPs (named NB@BPs) not only exhibit robust stability against rapid degradation in optical performance but also are endowed with strong NIR fluorescence. *In vitro* and *in vivo* experiments are performed to evaluate the applicability of the NB@BPs, inferring that NB@BPs can be used as multifunctional

DOI: 10.1021/acs.chemmater.7b01106
Chem. Mater. 2017, 29, 7131−7139

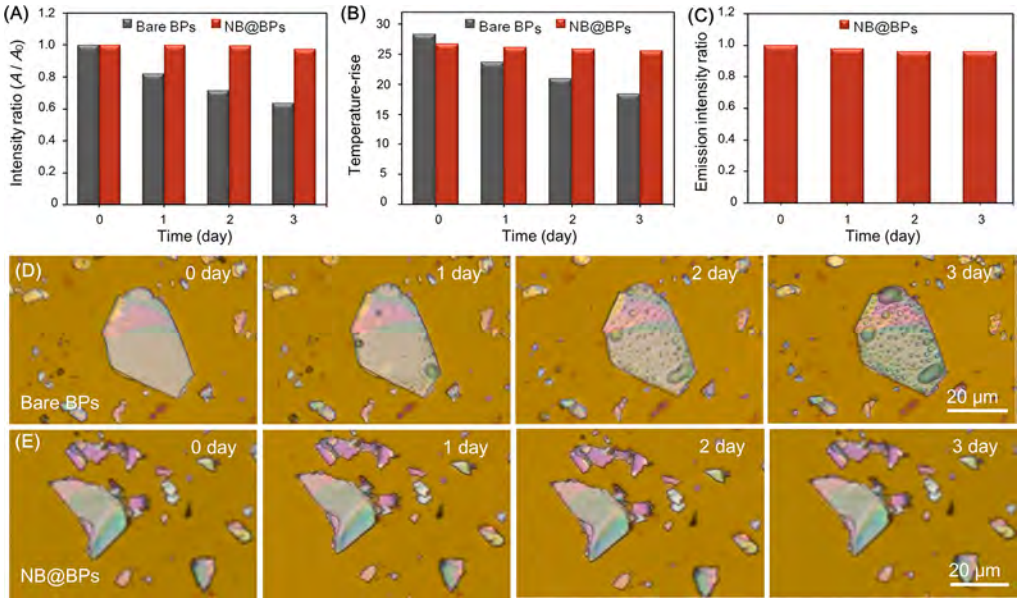

Figure 3. Stability examination. Time-dependent variations in the (A) absorption ratios at the respective peak wavelength (A/A_0) and (B) temperature increase of bare BPs and NB@BPs in water under 808 nm and 1.0 W cm^{-2} laser irradiation for 10 min. (C) Time-dependent variation in the fluorescence intensity of NB@BPs in water. Optical images of microsized (D) bare BPs and (E) NB@BPs exposed under ambient conditions for different dispersion times.

nanomedicine in imaging-guided photothermal therapy of cancer.

RESULTS AND DISCUSSION

Preparation and Characterizations of NB@BPs. A classical diazo reation is adopted to convert the free amino group of NB into the diazonium tetrafluoroborate salt to produce the fluorescent dye NB-D as shown in Figures S1−S4. NB-D exhibits characteristc Raman peaks at 591.2 and 673.4 cm^{-1} arising from the in-plane CCC, CNC, and NCC modes and other peaks at 344.0, 467.2, 497.5, and 750.2 cm^{-1} consistent with previous reports.[44,45] In the absorption spectrum, NB-D shows two typical peaks at 596 and 630 nm, and under 570 nm excitation, NIR fluorescence at ∼680 nm is observed, demonstrating that NB after diazonium tetrafluoroborate modification retains its fluorescence properties.

The BPs are synthesized in *N*-methyl-2-pyrrolidone (NMP) by a liquid exfoliation technique.[46] The transmission electron microscopy (TEM) images show that the average lateral size is ∼35.0 nm and the thickness is ∼6.0 nm, and high-resolution TEM (HR-TEM) reveals lattice fringers of 0.23 nm ascribed to the (014) plane of the BP crystal (see Figure S5). The exfoliated BPs react with NB-D via the covalent modification method as illustrated in Figure 1A. This reaction depends on the transfer of an electron from the surface of BPs to aryl diazonium ions to liberate N_2 and create a highly reactive aryl radical to form a covalent C−P bond.[41,47] After modificaiton, the NB@BPs are washed successively with acetonitrile, ethanol, and ultrapure water to remove the unbonded NB-D molecules. As shown in the TEM images in Figure 1B and Figure S5A, the NB-D modification has not changed the morphology and structure of the BPs, and the HR-TEM image reveals lattice fringes of 0.33 nm ascribed to the (021) plane of the BP crystal,[21] suggesting that the structure of BP is preserved after chemical modificaiton.

Covalent modification of BPs with NB-D is confirmed by high-resolution X-ray photoelectron spectroscopy (HR-XPS) in Figure 1C. The NB@BPs show the P $2p_{2/3}$ and P $2p_{1/2}$ doublets at 129.8 and 130.8 eV, respectively, characteristic of crystalline BP,[39] and the broad peak at 133.3 eV corresponds to phosphorus-aryl compounds,[41] corroborating formation of C−P covalent bonds. A P_xO_y sub-band emerges at 134.9 eV probably due to partial oxidation during synthesis and measurement.[26] As shown by the C 1s XPS spectra in Figure 1D, in addtion to C−O and C═O peaks at 284.8, 286.3, and 288.6 eV, the P−C peak at 284.2 eV[41] confirms the existence of the P−C bond.

Raman scattering is further performed, and as shown in Figure 1E, the bare BPs show three prominent Raman peaks related to out-of-plane phonon mode A^1_g at 361.5 cm^{-1} and in-plane modes B_{2g} and A^2_g at 438.2 and 466.0 cm^{-1}, respectively.[19] All the Raman peaks of BP and NB can be observed from NB@BPs.

Optical Properties of NB@BPs. Figure 2A shows the absorption spectra of bare BPs and NB@BPs dispersed in water. The bare BPs show a broad absorption band spanning the UV and NIR region, and for NB@BPs, additional NB absorption peaks due to integration of the two components are observed.

The photothermal properties of bare BPs and NB@BPs dispersed in water are determined with pure water as the control. The relationship between temperature and time is studied with 808 nm and 1.0 W cm^{-2} NIR laser irradiation. As shown by the photothermal heating curves in Figure 2B, the water solution containing either the bare BPs or NB@BPs (50 ppm) exhibits excellent photothermal conversion ability, and the temperature increases by ∼27.5 °C after 10 min compared to an increase of only 3.5 °C in pure water. The photothermal performance of NB@BPs is as good as that of bare BPs.

Although it has been reported that the mechanically exfoliated single-layer phosphorene can luminesce at ∼850 nm,[19] it is still difficult to observe fluorescence of liquid exfoliated BPs particularly when they are dispersed in solution. In our study, the fluorescence properties of bare BPs and NB@

DOI: 10.1021/acs.chemmater.7b01106
Chem. Mater. 2017, 29, 7131−7139

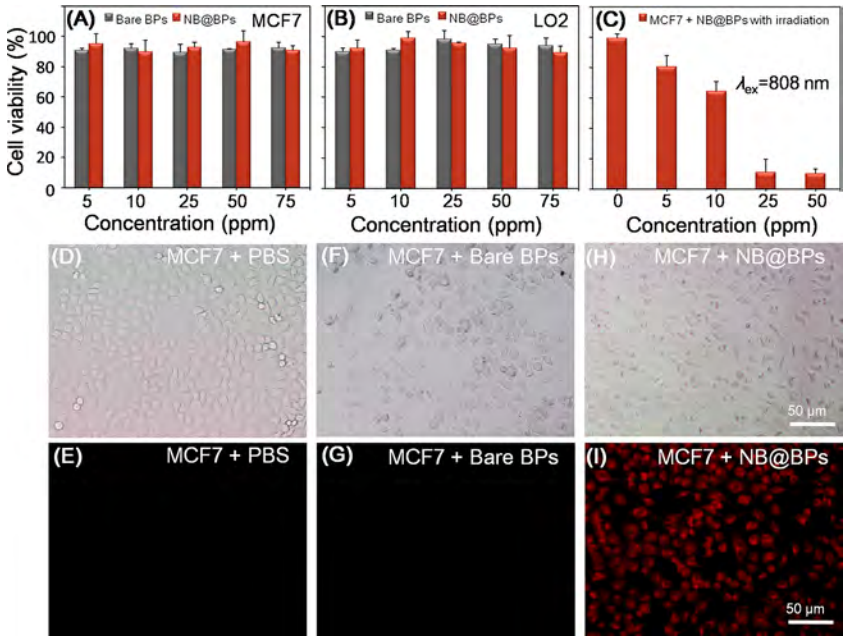

Figure 4. *In vitro* cell culture performance. Relative cell viabilities of (A) MCF7 cells and (B) LO2 cells incubated with bare BPs and NB@BPs at different concentrations (5, 10, 25, 50, and 75 ppm). (C) Relative viabilities of MCF7 cells incubated with different concentrations of NB@BPs after irradiation with an 808 nm and 1.0 W cm^{-2} laser for 10 min. (D, F, and H) White light images and (E, G, and I) corresponding fluorescence images of MCF7 cells incubated with PBS, bare BPs, and NB@BPs, respectively.

BPs dispersed in water are determined, and the emission spectra (λ_{ex} = 570 nm) are shown in Figure 2C. The NB@BPs show typical NB NIR fluorescence at ∼680 nm. Figure 2D further demonstrates bright fluorescence from NB@BPs, whereas bare BPs do not fluoresce. To further investigate the fluorescence characteristics of NB@BPs, microsized BPs (see Figure S6) are synthesized by the liquid exfoliation method as well as NB modification as described above. Panels E and F of Figure 2 show the bright-field and fluorescnece images of the microsized NB@BPs, respectively. Intense red fluorescence can be directly observed from the microsized NB@BPs under 570 nm light excitation. These results demonstrate successful synthesis of fluorescent BPs by NB-D covalent modification, suggesting good potential as a light-activatable multifunctional agent.

Evaluation of the Stability of NB@BPs. To evaluate the role of NB-D covalent modification in BP stability, the bare BPs and NB@BPs are dispersed in water and exposed to air for 0, 1, 2, and 3 days. The time-dependent optical absorbance is monitored, and the variation in the A/A_0 absorption ratios at 630 nm is shown in Figure 3A. The absorbance intensity of the bare BPs decreases obviously with time, showing an ∼40% reduction after 3 days. Degradation of BPs depends on the reaction between P and oxygen (P → P_xO_y), and water facilitates conversion of P_xO_y to the final anions (i.e., PO_4^{3-}).[30] When the bare BPs are dispersed in water, quick removal of P_xO_y and continuous exposure of fresh P_0 to oxygen accelerate BP degradation, so the absorbance decreases continuously. In contrast, the absorbance of NB@BPs is maintained in water, and the peak absorbance intensity decreases by only 3% after 3 days.

The photothermal stabilities of the bare BPs and NB@BPs are compared. In particular, the increase in temperature with time is determined from the bare BPs and NB@BPs in water under 808 nm and 1.0 W cm^{-2} NIR laser illumination for 10 min. The time-dependent variation is shown in Figure 3B. With respect to the bare BPs, the original temperature increase is 28.3 °C and the temperature decreases to 18.4 °C after 3 days. In contrast, the temperature of the NB@BP solution increases by 25.3 °C after 3 days, which is close to the original value. The difference in the photothermal performance between the bare BPs and NB@BPs is consistent with the optical absorbance variations. As shown in Figure 3C, the fluorescence intensity of NB@BPs is stable in water for at least 3 days.

The microsized bare BPs and NB@BPs are placed on Si/SiO_2 substrates for further assessment of the stability under ambient conditions. Panels D and E of Figure 3 present the typical optical images after exposure to humid air for 0, 1, 2, and 3 days. Small water droplets are observed from the bare BPs after 1 day, and the droplets become larger and denser with time. These findings are consistent with the previously reported morphological changes on BP sheets in air.[29,48] In comparison, the microsized NB@BPs are almost unchanged after exposure to air for 3 days. The results demonstrate the efficacy of NB-D covalent modification in preventing BPs from rapidly degrading.

***In Vitro* Cytotoxicity Assays, Photothermal Effect, and Fluorescence Imaging.** Nanomaterials for application to biomedicine must be sufficiently biocompatible, so the cytocompatibility of the bare BPs and NB@BPs is evaluated. The standard Cell Counting Kit-8 (CCK-8) assay is performed to determine the relative viabilities of MCF7 breast cancer cells and LO2 normal cells when the cells are separately incubated with bare BPs and NB@BPs at different concentrations for 48 h. As shown in panels A and B of Figure 4, no cytotoxicity can be observed from the two types of cells even at a high concentration of 75 ppm, confirming the good biocompatibility and suitability of biomedical application.

In addition to the cytocompatibility assessment, the photothermal effects of the NB@BPs on cancer cells are examined (see Figure 4C). The MCF7 cancer cells are incubated with different concentrations of NB@BPs for 4 h,

DOI: 10.1021/acs.chemmater.7b01106
Chem. Mater. 2017, 29, 7131−7139

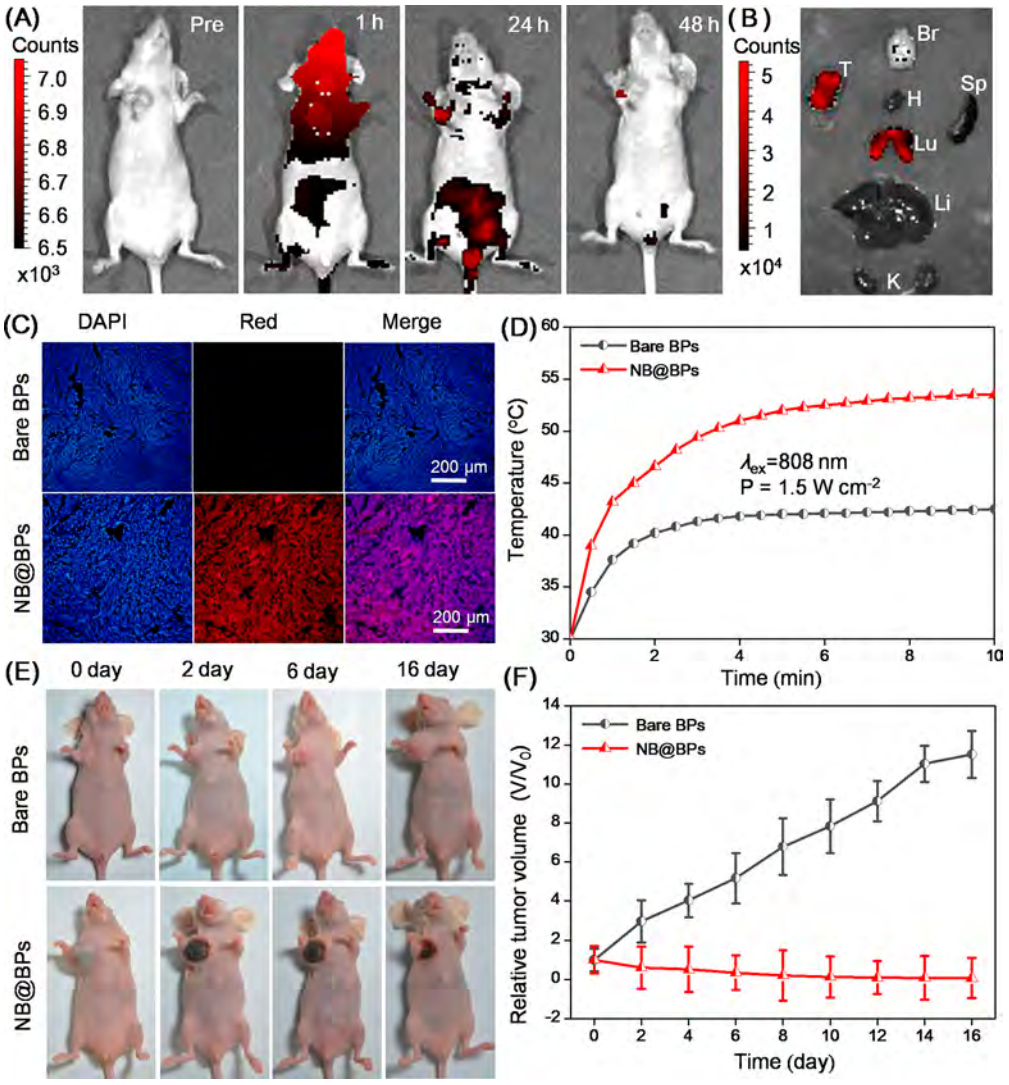

Figure 5. *In vivo* fluorescence bioimaging and photothermal therapy. (A) Fluorescence images of the MCF7 breast tumor-bearing nude mice treated with the NB@BPs via the tail vein at different time points postinjection. (B) Fluorescence images of the tumor and major organs from the mice treated with NB@BPs 1 h postinjection. Abbreviations: Br, brain; H, heart; Sp, spleen; Lu, lung; Li, liver; K, kidney; T, tumor. (C) Fluorescence micrographs of tumor sections from mice treated with BPs and NB@BPs. Red fluorescence refers to NB@BPs and blue fluorescence to nuclei stained with DAPI. (D) Time-dependent temperature increase. (E) Typical photograph. (F) Tumor growth curves of the MCF7 breast tumor-bearing nude mice irradiated by the 808 nm and 1.5 W cm^{-2} NIR laser for 10 min after intravenous injection of bare BPs and NB@BPs.

and the cells are illuminated with the NIR laser for 10 min. The CCK-8 assay is used to determine the relative cell viabilities after irradiation, and dose-dependent photothermal effects on MCF7 cells are observed. As shown in Figure 4C, ~90% of the cells are killed in the presence of only 50 ppm of NB@BPs after exposure to the NIR laser. It should be noted that when the dose of NB@BPs is only 50 ppm, the threshold of photothermal cell destruction using the 808 nm laser is 1.0 W cm^{-2} for 10 min. These conditions are more moderate than those required by other photothermal nanoagents for *in vitro* photothermal cell destruction.[49,50]

The cell staining capability of fluorescent NB@BPs is also evaluated. In brief, the MCF7 cancer cells are incubated with PBS, bare BPs, and NB@BPs for 4 h and examined by fluorescence microscopy. Panels D−I of Figure 4 show that the cells incubated with NB@BPs exhibit intense fluorescence under 570 nm light excitation, but no fluorescence can be observed from the PBS and bare BP groups. These results demonstrate that the NB@BPs are capable of labeling cancer cells with bright NIR fluorescence. Moreover, a co-staining experiment using Hoechst 33528 is performed to determine the destination of internalized NB@BPs. As shown in Figure S7, strong red fluorescence signals from NB@BPs appear mainly in the cytoplasm of cells, whereas little red fluorescence is found in nuclei, which is co-stained blue by Hoechst. These results suggest that the internalized NB@BPs are mainly distributed in the cytoplasm.

To explore the cellular uptake process of NB@BPs, the endocytosis process is studied. Generally, external nanomaterials can enter into cells mainly through three types of endocytosis processes: (a) caveolae-mediated endocytosis, (b) clathrin-mediated endocytosis, and (c) macropinocytosis.[51] Thus, we investigated these processes individually by different endocytosis inhibitors, including methyl-β-cyclodextrin (mβCD), sucrose, and amiloride, which inhibit caveolae-mediated endocytosis, clathrin-mediated endocytosis, and macropinocytosis, respectively. As shown in Figure S8, the intracellular intensity of red fluorescence from NB@BPs is

DOI: 10.1021/acs.chemmater.7b01106
Chem. Mater. 2017, 29, 7131−7139

significantly decreased upon treatment with amiloride, indicating that the endocytosis of NB@BPs is mainly mediated by the micropinocytosis process.

***In Vivo* Fluorescence Imaging and Photothermal Therapy.** *In vivo* experiments are performed to evaluate the bioimaging capability of the NB@BPs. Briefly, Balb/c nude mice bearing the MCF7 breast tumors are treated with the solution of NB@BPs via the tail vein (100 μL of a solution of 1 mg of BP mL^{-1}) and examined by fluorescence imaging (see Figure 5A). Compared with the disorganized fluorescence signal distribution 1 h postinjection, considerable fluorescence signals can be observed from the tumor and some organs 24 h postinjection. Forty-eight hours postinjection, the fluorescence signal fades almost completely, suggesting clearance of NB@BPs from the body through the reticuloendothelial system (RES).

Figure 5B shows the typical *ex vivo* fluorescence images obtained 1 h postinjection. NB fluorescence can be observed mainly from the tumor and lung at this time point. Cryosections of the tissue are further studied by using DAPI to stain the nuclei blue (see Figure 5C). As expected, no fluorescence can be observed from bare BP groups, whereas NB@BPs exhibit strong NIR fluorescence in the tumor section. These results confirm that the NB@BPs can penetrate the tumor cells producing fluorescence from the tumor region.

The fluorescence intensity in blood is further examined by fluorometry at different time intervals postinjection, and the change in the intensity ratio (A/A_0) is plotted in Figure S9, in which A and A_0 are the fluorescence intensities at time t and 0 h postinjection, respectively. The blood circulation of NB@BPs obeys the typical two-compartment model. After the rapid distribution phase (first phase) with a half-life of ∼3.3 h, the fluorescence intensity in the circulating blood shows an elimination phase (second phase that is the predominant process for the clearance of NB@BPs) with a half-life of ∼15.5 h. The bioimaging results reveal bright NIR fluorescence from NB@BPs and considerable uptake of the nanoagents by the tumor because of the enhanced permeability and retention (EPR) effects. Because P is abundant in organisms, it is very difficult to trace the biodistribution of bare BPs.[52] Nonetheless, the NB@BPs with bright NIR fluorescence properties after NB modification enable non-invasive monitoring of the agent in animals.

To evaluate the potential of NB@BPs in photothermal cancer therapy, the Balb/c nude mice bearing the MCF7 breast tumors are successively treated via the tail vein with 100 μL of bare BPs and NB@BPs (1 mg of BP mL^{-1}), and then the entire region of the tumor is irradiated with the 808 nm laser (1.5 W cm^{-2}) for 10 min 1 h postinjection. As shown in Figure 5D, the tumor temperature of the mice treated with NB@BPs increases by 23.5 °C under NIR laser irradiation and is high enough for tumor ablation. On the other hand, the tumor temparature of the mice treated with BPs increases by only 11.5 °C, which may be attributed to rapid degradation of bare BPs during blood circulation. These results indicate the high efficiency of NB@BPs as a photothermal therapy agent during *in vivo* tumor ablation.

After the photothermal treatment, the tumor size is determined every 2 days, and no obvious toxic side effects such as abnormal body weight, activity, eating, drinking, or neurological issues can be observed in the two groups. As shown in panels E and F of Figure 5, the tumors in the mice treated with NB@BPs shrink gradually and are completely cured within 16 days. In contrast, tumor growth in the mice treated with BPs does not abrade. These results demonstrate the high efficacy of NB@BPs in NIR photothermal cancer therapy.

CONCLUSION

In summary, a NB diazonium tetrafluoroborate salt is synthesized to covalently modify BPs by aryl diazonium chemistry to produce stable and fluorescent NB@BPs for NIR imaging-guided photothermal cancer therapy. In contrast to serious degradation of bare BPs, NB@BPs show bright NIR fluorescence and inappreciable degradation of their optical properties. *In vitro* experiments demonstrate that the BPs after NB-D covalent modification are nontoxic. As a result of the stable NIR fluorescence and photothermal characteristics, the NB@BPs are successfully used in both NIR fluorescence imaging and photothermal tumor ablation during *in vivo* experiments. This effective and simple method enhances the stability of BPs and also endows the materials with multiple functions, spurring potential biological and biomedical applications.

EXPERIMENTAL SECTION

Materials. The BP crystals were purchased from a commercial supplier (Smart-Elements) and stored in a dark Ar glovebox. NMP (99.5%, anhydrous), ethanol (EtOH), sodium nitrite ($NaNO_2$), and hydrochloric acid (HCl) were obtained from Aladdin Reagents, and acetonitrile (CH_3CN, 99.9% anhydrous) and tetrafluoroborate (HBF_4) were obtained from Alfa-Aesar. Nile Blue 690 and tetrabutylammonium hexafluorophosphate ($[Bu_4N]^+PF_6^-$) were obtained from Sigma-Aldrich. All the chemicals were analytical reagent grade and used without further purification.

Synthesis of NB-D. One milliliter of 2.75 mmol of $NaNO_2$ was added dropwise to an ice-cold mixture of Nile Blue 690 (1 mmol) in 13% HCl (2.5 mL, 1 mmol). After the mixture had been stirred for 1 h at 0 °C, 50% HBF_4 (240 μL, 1.5 mmol) was added, and the mixture was stirred for an additional hour at 0 °C. The mixture was filtered and washed with cold water and then cold methanol. After the mixture had dried at room temperature, dark blue powders were obtained: ^{1}H NMR (400 MHz, DMSO) δ_H 8.73 (t, 1H, J = 8.0 Hz), 8.41 (t, 1H, J = 8.0 Hz), 7.96 (q, 1H), 7.87−7.75 (m, 2H), 7.22 (t, 1H, J = 8.0 Hz), 8.95 (d, 1H, J = 8.0 Hz), 8.79 (d, 1H, J = 8.0 Hz), 3.66 (q, 4H), 1.24 (t, 6H); ^{13}C NMR (100 MHz, DMSO) δ 161.2, 154.0, 153.4, 148.1, 133.4, 132.9, 132.8, 131.7, 130.0, 129.6, 124.5, 124.3, 122.9, 115.5, 97.0, 96.3, 45.8, 13.1; HRMS $(M - N_2)^+$ $C_{20}H_{19}N_2O^+$ calcd 303.1497, found 303.1491.

Synthesis of BP Nanosheets (BPs). The BPs were synthesized by a liquid exfoliation method. In brief, 20 mg of the bulk BP powders was dispersed in 20 mL of NMP and sonicated with a sonic tip (ultrasonic frequency of 19−25 kHz) for 5 h (period of 2 s with an interval of 4 s) using a power of 1200 W. The mixture was sonicated for 8 h in an ice bath using a power of 300 W. The dispersion was centrifuged for 20 min at 4000 rpm, and the collected supernatant was centrifuged for 20 min at 7000 rpm. The supernatant containing the BPs was decanted gently.

Synthesis of NB@BPs. A proper amount of NB-D with $[Bu_4N]^+PF_6^-$ was added to the BP solution in CH_3CN (for 100 μg of BP in 1 mL of CH_3CN, add 1 mL of a 10 mg/mL NB-D solution in CH_3CN), and the mixture was stirred in darkness under nitrogen for 20 h. The mixture was centrifuged at 7000 rpm for 10 min, and the residue was washed with CH_3CN (2 mL), ethanol (2 mL), and water (2 mL) twice successively. After the wash, the NB@BPs were resuspended in ethanol or water. For subsequent experiments, the solution was centrifuged at 7000 rpm for 10 min and the precipitated NB@BPs were collected.

Characterization. The TEM and HR-TEM images were recorded on the Tecnai G2 F20 S-Twin transmission electron microscope at an

DOI: 10.1021/acs.chemmater.7b01106
Chem. Mater. 2017, 29, 7131−7139

acceleration voltage of 200 kV. Raman scattering was conducted on a Horiba Jobin-Yvon Lab Ram HR VIS high-resolution confocal Raman microscope equipped with a 633 nm laser. XPS was conducted on the Thermo Fisher Escalab250Xi XPS instrument 3 days after samples were placed on the Si/SiO_2 substrate. The ultraviolet−visible−NIR absorption spectra were recorded at room temperature on the Hitachi U-3900 spectrophotometer with QS-grade quartz cuvettes, and the fluorescence spectra were recorded on the Hitachi F-4600 spectrophotometer. The optical images of the Si/SiO_2 substrates were recorded on the Keyence VHX-2000C optical microscope. The *in vitro* fluorescence images were recorded on the Olympus-BX63 fluorescence microscope, and the *in vivo* fluorescence images were recorded for the mice using the Caliper Ivis Spectrum imaging system.

NIR Laser-Induced Heat Conversion. A 1 cm path length quartz cuvette containing 0.5 mL of the bare BPs or NB@BPs was covered with a foam cap. The cuvette was clamped on the top part above the sample surface, and the bottom of the cuvette was kept ∼0.5 cm above the magnetic stirrer. A continuous fiber-coupled semiconductor diode laser (808 nm, KS-810F-8000, Kai Site Electronic Technology Co., Ltd., Shanxi, China) with a power density of 1.0 W cm^{-2} was employed as the light source, and an infrared thermal imaging camera (Fluke Ti27) was used to monitor the temperature change.

Cellular Toxicity Assay. The MCF7 breast cancer cells were obtained from China type culture collection (CTCC). The cells were cultured on a 96-well plate (1×10^4 cells/well) in Dulbecco's modified Eagle's medium (Gibco BRL) supplemented with 10% (v/v) fetal bovine serum, 100 IU mL^{-1} penicillin, and 100 IU mL^{-1} streptomycin in a humid atmosphere of 5% CO_2 at 37 °C. After 12 h, the DMEM was replaced with 200 μL of the DMEM containing 20 μL of the desired sample per well (bare BPs and NB@BPs at different concentrations of 5, 10, 25, 50, and 75 ppm). Five multiple holes were set for every sample. The cells were treated with the samples for 48 h, and then the cell viability was assayed by adding 10 μL of a CCK-8 solution to each well. After the cells were incubated with CCK-8 at 37 °C for 2 h, the absorbance that correlated with the number of viable cells in each well was determined on a Thermo Reader at 450 nm. The following formula was used to calculate the inhibition of cell growth: cell viability (%) = (mean of the absorbance value of the treatment group/mean absorbance value of the control) × 100%.

***In Vitro* Photothermal and Fluorescence Imaging Experiments.** To determine the photothermal efficacy of NB@BPs, the standard CCK-8 assay was employed to determine the relative viability of the MCF7 cancer cells. The cell viability was normalized to the control group without any treatment. In particular, the MCF7 cells (1×10^4 cells/well) were seeded on 96-well plates and incubated in a humidified atmosphere of 5% CO_2 at 37 °C overnight. The MCF7 cells were rinsed twice with PBS (pH 7.4) and incubated without and with NB@BPs for 4 h. The fluorescent ability of the NB@BPs to label the MCF7 cells is evaluated on the Olympus-BX63 fluorescence microscope. In the photothermal experiments, the cells were irradiated with the 808 nm laser (1.0 W cm^{-2}) for 10 min. The laser spot was adjusted to fully cover the area of each well. After being illuminated, the cells were incubated for 12 h, and the cell viability was determined by the same CCK-8 assay as mentioned above.

***In Vivo* Fluorescence Imaging and Photothermal Experiments.** The healthy female Balb/c nude mice (6 weeks old) were obtained from Slac Laboratory Animal Co. Ltd. (Hunan, China), and all the *in vivo* experiments followed the protocols approved by the Animal Care and Use Committee of the Shenzhen Institutes of Advanced Technology, Chinese Academy of Sciences. To establish the MCF7 breast tumors *in situ* in the Balb/c nude mouse, 1×10^7 MCF7 cells in 100 μL of PBS were subcutaneously injected into the left foreleg armpit of each mouse. When the tumor volume reached 200 mm^3, the mice were randomly divided into two groups (n = 3 per group), and aliquots (100 mL) of bare BPs and NB@BPs (1 mg of BP mL^{-1}) were injected separately into the nude mice intratumorally. The fluorescent ability of NB@BPs to label tumors in the mice was evaluated by the Caliper Ivis Spectrum imaging system at the indicated times.

In the *ex vivo* fluorescence imaging experiments, the mice treated with NB@BPs were killed by cervical dislocation and the corresponding major organs and tissues, including the liver, spleen, kidney, heart, stomach, lung, intestine, and tumor, were collected and imaged. The tumors were fixed in a 4% polyformaldehyde fixing solution and embedded in a 30% aqueous sucrose solution. Sections of the whole tumor were stained using DAPI (colored blue) to label all nuclei of the tumor cells. The fluorescence images of the tumor sections were obtained on an Olympus-BX63 fluorescence microscope. As part of the blood analysis, blood circulation was assessed by drawing 10 μL of blood from the tail vein of the Balb/c nude mice at certain time intervals after injection of the NB@BPs. Each blood sample was dissolved in 1 mL of lysis buffer (cell lysis buffer for Western and immunol precipitation, Beyotime biotechnology); the fluorescence intensity of the blood was determined from the fluorescence spectrum recorded on a Fluoromax 4 fluorometer (Horiba Jobin Yvon), and the A/A_0 values were calculated.

To evaluate the photothermal potential of the NB@BPs, the mice were anesthetized 0.5 h postinjection, and the entire region of the tumor was irradiated with the 808 nm and 1.5 W cm^{-2} NIR laser for 10 min. The temperature of the tumors was recorded by an infrared thermal imaging camera (Ti27, Fluka). After laser irradiation, the tumor size was measured by a caliper every 2 days according to the formula volume (V) = (tumor length)(tumor width)^2/2, and no mouse died during the course of therapy. The relative tumor volume was calculated as V/V_0, with V_0 being the initial tumor volume at the start of the treatment. Daily clinical observations, including weekends and holidays, were performed to monitor the animals for signs of distress. When the tumor size reached 20 mm in any direction or the mouse displayed restriction, inability to access food or water, or pressure on internal organs or sensitive regions of the body, the mice were euthanized.

■ ASSOCIATED CONTENT

Supporting Information

The Supporting Information is available free of charge on the ACS Publications website at DOI: 10.1021/acs.chemmater.7b01106.

Optical characterization and ^1H nuclear magnetic resonance, ^{13}C nuclear magnetic resonance, and mass spectra of NB-D; characterization of BPs; TEM image of microsized BPs; confocal images of MCF7 cells with NB@BPs; inhibition of endocytosis with different inhibitors of NB@BPs for cellular uptake; and fluorescence intensity ratios (A/A_0) in blood at different time points after injection of the NB@BPs (PDF)

■ AUTHOR INFORMATION

Corresponding Author

*E-mail: xf.yu@siat.ac.cn.

ORCID

Xue-Feng Yu: 0000-0003-2566-6194

Notes

The authors declare no competing financial interest.

■ ACKNOWLEDGMENTS

This work was jointly supported by the National Natural Science Fund of China (51672305 and 51503220), the Frontier Research Key Project of the Chinese Academy of Sciences (QYZDB-SSW-SLH034), Shenzhen Science and Technology Research Funding (JCYJ20160229195124187 and JCYJ20160429190215470), Leading Talents of Guangdong Province Program 00201520, and Hong Kong Research Grants Council (RGC) General Research Funds (GRF) (11301215).

DOI: 10.1021/acs.chemmater.7b01106
Chem. Mater. 2017, 29, 7131−7139

REFERENCES

(1) Weissleder, R. A Clearer Vision for *in vivo* Imaging. *Nat. Biotechnol.* **2001**, *19*, 316−317.

(2) Rao, L.; Bu, L. L.; Cai, B.; Xu, J. H.; Li, A.; Zhang, W. F.; Sun, Z. J.; Guo, S. S.; Liu, W.; Wang, T. H.; Zhao, X. Z. Cancer Cell Membrane-Coated Upconversion Nanoprobes for Highly Specific Tumor Imaging. *Adv. Mater.* **2016**, *28*, 3460−3466.

(3) Wang, Y. H.; Wang, H. G.; Liu, D. P.; Song, S. Y.; Wang, X.; Zhang, H. J. Graphene Oxide Covalently Grafted Upconversion Nanoparticles for Combined NIR Mediated Imaging and Photothermal/Photodynamic Cancer Therapy. *Biomaterials* **2013**, *34*, 7715−7724.

(4) Tian, Q. W.; Tang, M. H.; Sun, Y. G.; Zou, R. J.; Chen, Z. G.; Zhu, M. F.; Yang, S. P.; Wang, J. L.; Wang, J. H.; Hu, J. Q. Hydrophilic Flower-Like CuS Superstructures as an Efficient 980 nm Laser-Driven Photothermal Agent for Ablation of Cancer Cells. *Adv. Mater.* **2011**, *23*, 3542−3547.

(5) Yang, K.; Hu, L. L.; Ma, X. X.; Ye, S. Q.; Cheng, L.; Shi, X. Z.; Li, C. H.; Li, Y. G.; Liu, Z. Multimodal Imaging Guided Photothermal Therapy using Functionalized Graphene Nanosheets Anchored with Magnetic Nanoparticles. *Adv. Mater.* **2012**, *24*, 1868−1872.

(6) Sang, Y. H.; Zhao, Z. H.; Zhao, M. W.; Hao, P.; Leng, Y. H.; Liu, H. From UV to Near-Infrared, WS2 Nanosheet: A Novel Photocatalyst for Full Solar Light Spectrum Photodegradation. *Adv. Mater.* **2015**, *27*, 363−369.

(7) Zhu, C. Q.; Yang, Y. H.; Luo, M.; Yang, C. X.; Wu, J. J.; Chen, L. N.; Liu, G.; Wen, T. B.; Zhu, J.; Xia, H. P. Stabilizing Two Classical Antiaromatic Frameworks: Demonstration of Photoacoustic Imaging and the Photothermal Effect in Metalla-aromatics. *Angew. Chem., Int. Ed.* **2015**, *54*, 6181−6185.

(8) Hirsch, L. R.; Stafford, R. J.; Bankson, J. A.; Sershen, S. R.; Rivera, B.; Price, R. E.; Hazle, J. D.; Halas, N. J.; West, J. L. Nanoshell-Mediated Near-Infrared Thermal Therapy of Tumors under Magnetic Resonance Guidance. *Proc. Natl. Acad. Sci. U. S. A.* **2003**, *100*, 13549−13554.

(9) Hauck, T. S.; Jennings, T. L.; Yatsenko, T.; Kumaradas, J. C.; Chan, W. C. W. Enhancing the Toxicity of Cancer Chemotherapeutics with Gold Nanorod Hyperthermia. *Adv. Mater.* **2008**, *20*, 3832−3838.

(10) Dong, K.; Liu, Z.; Li, Z. H.; Ren, J. S.; Qu, X. G. Hydrophobic Anticancer Drug Delivery by a 980 nm Laser-Driven Photothermal Vehicle for Efficient Synergistic Therapy of Cancer Cells *in vivo*. *Adv. Mater.* **2013**, *25*, 4452−4458.

(11) Yin, W. Y.; Yan, L.; Yu, J.; Tian, G.; Zhou, L. J.; Zheng, X. P.; Zhang, X.; Yong, Y.; Li, J.; Gu, Z. J.; Zhao, Y. L. High-Throughput Synthesis of Single-Layer MoS_2 Nanosheets as a Near-Infrared Photothermal-Triggered Drug Delivery for Effective Cancer Therapy. *ACS Nano* **2014**, *8*, 6922−6933.

(12) Shi Kam, N. W.; O'Connell, M.; Wisdom, J. A.; Dai, H. J. Carbon Nanotubes as Multifunctional Biological Transporters and Near-Infrared Agents for Selective Cancer Cell Destruction. *Proc. Natl. Acad. Sci. U. S. A.* **2005**, *102*, 11600−11605.

(13) Wang, S. H.; Shang, L.; Li, L. L.; Yu, Y. J.; Chi, C. W.; Wang, K.; Zhang, J.; Shi, R.; Shen, H. Y.; Waterhouse, G. I. N.; Liu, S. J.; Tian, J.; Zhang, T. R.; Liu, H. Y. Metal-Organic-Framework-Derived Mesoporous Carbon Nanospheres Containing Porphyrin-Like Metal Centers for Conformal Phototherapy. *Adv. Mater.* **2016**, *28*, 8379−8387.

(14) Li, B.; Ye, K. C.; Zhang, Y. X.; Qin, J. B.; Zou, R. J.; Xu, K. B.; Huang, X. J.; Xiao, Z. Y.; Zhang, W. J.; Lu, X. W.; Hu, J. Q. Photothermal Theragnosis Synergistic Therapy Based on Bimetal Sulphide Nanocrystals Rather Than Nanocomposites. *Adv. Mater.* **2015**, *27*, 1339−1345.

(15) Huang, X. H.; Neretina, S.; El-Sayed, M. A. Gold Nanorods: From Synthesis and Properties to Biological and Biomedical Applications. *Adv. Mater.* **2009**, *21*, 4880−4910.

(16) Liu, H.; Du, Y. C.; Deng, Y. X.; Ye, P. D. Semiconducting Black Phosphorus: Synthesis, Transport Properties and Electronic Applications. *Chem. Soc. Rev.* **2015**, *44*, 2732−2743.

(17) Yavuz, M. S.; Cheng, Y. Y.; Chen, J. Y.; Cobley, C. M.; Zhang, Q.; Rycenga, M.; Xie, J. W.; Kim, C.; Song, K. H.; Schwartz, A. G.; Wang, L. V.; Xia, Y. N. Gold Nanocages Covered by Smart Polymers for Controlled Release with Near-Infrared Light. *Nat. Mater.* **2009**, *8*, 935−939.

(18) Cheng, L.; Wang, C.; Feng, L.; Yang, K.; Liu, Z. Functional Nanomaterials for Phototherapies of Cancer. *Chem. Rev.* **2014**, *114*, 10869−10939.

(19) Liu, H.; Neal, A. T.; Zhu, Z.; Luo, Z.; Xu, X. F.; Tománek, D.; Ye, P. D. Phosphorene: An Unexplored 2D Semiconductor with a High Hole Mobility. *ACS Nano* **2014**, *8*, 4033−4041.

(20) Brent, J. R.; Savjani, N.; Lewis, E. A.; Haigh, S. J.; Lewis, D. J.; O'Brien, P. Production of Few-Layer Phosphorene by Liquid Exfoliation of Black Phosphorus. *Chem. Commun.* **2014**, *50*, 13338−13341.

(21) Yasaei, P.; Kumar, B.; Foroozan, T.; Wang, C. H.; Asadi, M.; Tuschel, D.; Indacochea, J. E.; Klie, R. F.; Salehi-Khojin, A. High-Quality Black Phosphorus Atomic Layers by Liquid-Phase Exfoliation. *Adv. Mater.* **2015**, *27*, 1887−1892.

(22) Kang, J.; Wood, J. D.; Wells, S. A.; Lee, J. H.; Liu, X. L.; Chen, K. S.; Hersam, M. C. Solvent Exfoliation of Electronic-Grade, Two-Dimensional Black Phosphorus. *ACS Nano* **2015**, *9*, 3596−3604.

(23) Woomer, A. H.; Farnsworth, T. W.; Hu, J.; Wells, R. A.; Donley, C. L.; Warren, S. C. Phosphorene: Synthesis, Scale-Up, and Quantitative Optical Spectroscopy. *ACS Nano* **2015**, *9*, 8869−8884.

(24) Zhang, X.; Xie, H. M.; Liu, Z. D.; Tan, C. L.; Luo, Z. M.; Li, H.; Lin, J. D.; Sun, L. Q.; Chen, W.; Xu, Z. C.; Xie, L. H.; Huang, W.; Zhang, H. Black Phosphorus Quantum Dots. *Angew. Chem., Int. Ed.* **2015**, *54*, 3653−3657.

(25) Lin, S. H.; Liu, S. H.; Yang, Z. B.; Li, Y. Y.; Ng, T. W.; Xu, Z. Q.; Bao, Q. L.; Hao, J. H.; Lee, C.-S.; Surya, C.; Yan, F.; Lau, S. P. Solution-Processable Ultrathin Black Phosphorus as an Effective Electron Transport Layer in Organic Photovoltaics. *Adv. Funct. Mater.* **2016**, *26*, 864−871.

(26) Sun, Z. B.; Xie, H. H.; Tang, S. Y.; Yu, X. F.; Guo, Z. N.; Shao, J. D.; Zhang, H.; Huang, H.; Wang, H. Y.; Chu, P. K. Ultrasmall Black Phosphorus Quantum Dots: Synthesis and Use as Photothermal Agents. *Angew. Chem., Int. Ed.* **2015**, *54*, 11526−11530.

(27) Wang, H.; Yang, X. Z.; Shao, W.; Chen, S. C.; Xie, J. F.; Zhang, X. D.; Wang, J.; Xie, Y. Ultrathin Black Phosphorus Nanosheets for Efficient Singlet Oxygen Generation. *J. Am. Chem. Soc.* **2015**, *137*, 11376−11382.

(28) Tao, W.; Zhu, X. B.; Yu, X. H.; Zeng, X. W.; Xiao, Q. L.; Zhang, X. D.; Ji, X. Y.; Wang, X. S.; Shi, J. J.; Zhang, H.; Mei, L. Black Phosphorus Nanosheets as a Robust Delivery Platform for Cancer Theranostics. *Adv. Mater.* **2017**, *29*, 1603276.

(29) Huang, Y.; Qiao, J. S.; He, K.; Bliznakov, S.; Sutter, E.; Chen, X. J.; Luo, D.; Meng, F.; Su, D.; Decker, J.; Ji, W.; Ruoff, R. S.; Sutter, T. Interaction of Black Phosphorus with Oxygen and Water. *Chem. Mater.* **2016**, *28*, 8330−8339.

(30) Wang, G. X.; Slough, W. J.; Pandey, R.; Karna, S. P. Degradation of Phosphorene in Air: Understanding at Atomic Level. *2D Mater.* **2016**, *3*, 025011.

(31) Ling, X.; Wang, H.; Huang, S. X.; Xia, F. N.; Dresselhaus, M. S. The Renaissance of Black Phosphorus. *Proc. Natl. Acad. Sci. U. S. A.* **2015**, *112*, 4523−4530.

(32) Comber, S.; Gardner, M.; Georges, K.; Blackwood, D.; Gilmour, D. Domestic Source of Phosphorus to Sewage Treatment Works. *Environ. Technol.* **2013**, *34*, 1349−1358.

(33) Childers, D. L.; Corman, J.; Edwards, M.; Elser, J. J. Sustainability Challenges of Phosphorus and Food: Solutions from Closing the Human Phosphorus Cycle. *BioScience* **2011**, *61*, 117−124.

(34) Pravst, I. Risking Public Health by Approving Some Health Claims? The Case of Phosphorus. *Food Policy* **2011**, *36*, 726−728.

(35) Favron, A.; Gaufrès, E.; Fossard, F.; Phaneuf-L'Heureux, A.-L.; Tang, N. Y. W.; Lévesque, P. L.; Loiseau, A.; Leonelli, R.; Francoeur, S.; Martel, R. Photooxidation and Quantum Confinement Effects in Exfoliated Black Phosphorus. *Nat. Mater.* **2015**, *14*, 826−832.

DOI: 10.1021/acs.chemmater.7b01106
Chem. Mater. 2017, 29, 7131−7139

(36) Kim, J. S.; Liu, Y.; Zhu, W.; Kim, S.; Wu, D.; Tao, L.; Dodabalapur, A.; Lai, K.; Akinwande, D. Toward Air-Stable Multilayer Phosphorene Thin-Films and Transistors. *Sci. Rep.* **2015**, *5*, 8989.
(37) Avsar, A.; Vera-Marun, I. J.; Tan, J. Y.; Watanabe, K.; Taniguchi, T.; Castro Neto, A. H.; Özyilmaz, B. Air-Stable Transport in Graphene-Contacted, Fully Encapsulated Ultrathin Black Phosphorus-Based Field-Effect Transistors. *ACS Nano* **2015**, *9*, 4138−4145.
(38) Wood, J. D.; Wells, S. A.; Jariwala, D.; Chen, K. S.; Cho, E. K.; Sangwan, V. K.; Liu, X. L.; Lauhon, L. J.; Marks, T. J.; Hersam, M. C. Effective Passivation of Exfoliated Black Phosphorus Transistors against Ambient Degradation. *Nano Lett.* **2014**, *14*, 6964−6970.
(39) Zhao, Y. T.; Wang, H. Y.; Huang, H.; Xiao, Q. L.; Xu, Y. H.; Guo, Z. N.; Xie, H. H.; Shao, J. D.; Sun, Z. B.; Han, W. J.; Yu, X.-F.; Li, P. H.; Chu, P. K. Surface Coordination of Black Phosphorus for Robust Air and Water Stability. *Angew. Chem., Int. Ed.* **2016**, *55*, 5003−5008.
(40) Abellán, G.; Lloret, V.; Mundloch, U.; Marcia, M.; Neiss, C.; Gorling, A.; Varela, M.; Hauke, F.; Hirsch, A. Noncovalent Functionalization of Black Phosphorus. *Angew. Chem., Int. Ed.* **2016**, *55*, 14557−14562.
(41) Ryder, C. R.; Wood, J. D.; Wells, S. A.; Yang, Y.; Jariwala, D.; Marks, T. J.; Schatz, G. C.; Hersam, M. C. Covalent Functionalization and Passivation of Exfoliated Black Phosphorus *via* Aryl Diazonium Chemistry. *Nat. Chem.* **2016**, *8*, 597−602.
(42) Yang, B. C.; Wan, B. S.; Zhou, Q. H.; Wang, Y.; Hu, W. T.; Lv, W. M.; Chen, Q.; Zeng, Z. M.; Wen, F. S.; Xiang, J. Y.; Yuan, S. J.; Wang, J. L.; Zhang, B. S.; Wang, W. H.; Zhang, J. Y.; Xu, B.; Zhao, Z. S.; Tian, Y. J.; Liu, Z. Y. Te-Doped Black Phosphorus Field-Effect Transistors. *Adv. Mater.* **2016**, *28*, 9408−9415.
(43) Zhao, Y. H.; Zhou, Q. H.; Li, Q.; Yao, X. J.; Wang, J. L. Passivation of Black Phosphorus via Self-Assembled Organic Monolayers by van der Waals Epitaxy. *Adv. Mater.* **2017**, *29*, 1603990.
(44) Lawless, M. K.; Mathies, R. A. Excited-State Structure and Electronic Dephasing Time of Nile Blue from Absolute Resonance Raman Intensities. *J. Chem. Phys.* **1992**, *96*, 8037−8045.
(45) Mohaghegh, F.; Mazaheri Tehrani, A.; Materny, A. Investigation of the Chemical Enhancement Contribution to SERS Using a Kretschmann Arrangement. *J. Raman Spectrosc.* **2016**, *47*, 1029−1035.
(46) Guo, Z. N.; Zhang, H.; Lu, S. B.; Wang, Z. T.; Tang, S. Y.; Shao, J. D.; Sun, Z. B.; Xie, H. H.; Wang, H. Y.; Yu, X.-F.; Chu, P. K. From Black Phosphorus to Phosphorene: Basic Solvent Exfoliation, Evolution of Raman Scattering, and Applications to Ultrafast Photonics. *Adv. Funct. Mater.* **2015**, *25*, 6996−7002.
(47) Allongue, P.; Delamar, M.; Desbat, B.; Fagebaume, O.; Hitmi, R.; Pinson, J.; Savéant, J.-M. Covalent Modification of Carbon Surfaces by Aryl Radicals Generated from the Electrochemical Reduction of Diazonium Salts. *J. Am. Chem. Soc.* **1997**, *119*, 201−207.
(48) Ziletti, A.; Carvalho, A.; Campbell, D. K.; Coker, D. F.; Castro Neto, A. H. Oxygen Defects in Phosphorene. *Phys. Rev. Lett.* **2015**, *114*, 046801.
(49) Hessel, C. M.; Pattani, V. P.; Rasch, M.; Panthani, M. G.; Koo, B.; Tunnell, J. W.; Korgel, B. A. Copper Selenide Nanocrystals for Photothermal Therapy. *Nano Lett.* **2011**, *11*, 2560−2566.
(50) Melancon, M. P.; Lu, W.; Yang, Z.; Zhang, R.; Cheng, Z.; Elliot, A. M.; Stafford, J.; Olson, T.; Zhang, J. Z.; Li, C. *In vitro* and *in vivo* Targeting of Hollow Gold Nanoshells Directed at Epidermal Growth Factor Receptor for Photothermal Ablation Therapy. *Mol. Cancer Ther.* **2008**, *7*, 1730−1739.
(51) Li, S. X.; Wang, K. K.; Shi, Y. J.; Cui, Y. N.; Chen, B. L.; He, B.; Dai, W. B.; Zhang, H.; Wang, X. Q.; Zhong, C. L.; Wu, H. N.; Yang, Q. Y.; Zhang, Q. Novel Biological Functions of ZIF-NP as a Delivery Vehicle: High Pulmonary Accumulation, Favorable Biocompatibility, and Improved Therapeutic Outcome. *Adv. Funct. Mater.* **2016**, *26*, 2715−2727.
(52) Shao, J. D.; Xie, H. H.; Huang, H.; Li, Z. B.; Sun, Z. B.; Xu, Y. H.; Xiao, Q. L.; Yu, X.-F.; Zhao, Y. T.; Zhang, H.; Wang, H. Y.; Chu, P. K. Biodegradable Black Phosphorus-Based Nanospheres for *in vivo* Photothermal Cancer Therapy. *Nat. Commun.* **2016**, *7*, 12967.

DOI: 10.1021/acs.chemmater.7b01106
Chem. Mater. 2017, 29, 7131−7139

Stable and Multifunctional Dye-Modified Black Phosphorus Nanosheets for Near-Infrared Imaging-Guided Photothermal Therapy

Yuetao Zhao[†], Liping Tong[†], Zhibin Li[‡], Na Yang[†], Haidi Fu[†], Lie Wu[†], Haodong Cui[†], Wenhua Zhou[†], Jiahong Wang[†], Huaiyu Wang[†], Paul K. Chu[‡], and Xue-Feng Yu*[,†]

[†] Institute of Biomedicine and Biotechnology, Shenzhen Institutes of Advanced Technology, Chinese Academy of Sciences, Shenzhen 518055, P. R. China

[‡] Department of Physics and Materials Science, City University of Hong Kong, Tat Chee Avenue, Kowloon, Hong Kong, China

E-mail: xf.yu@siat.ac.cn (X. F. Yu)

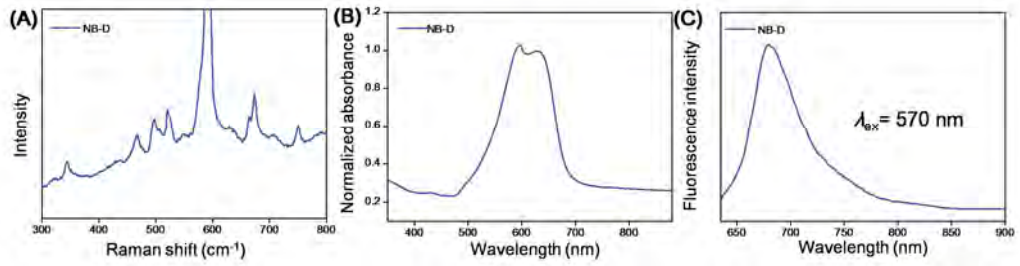

Figure S1. Optical characterization of NB-D: (A) Raman spectra, (B) Absorption spectra and (C) Fluorescence emission spectra (λ_{ex} = 570 nm) of water solution containing NB-D.

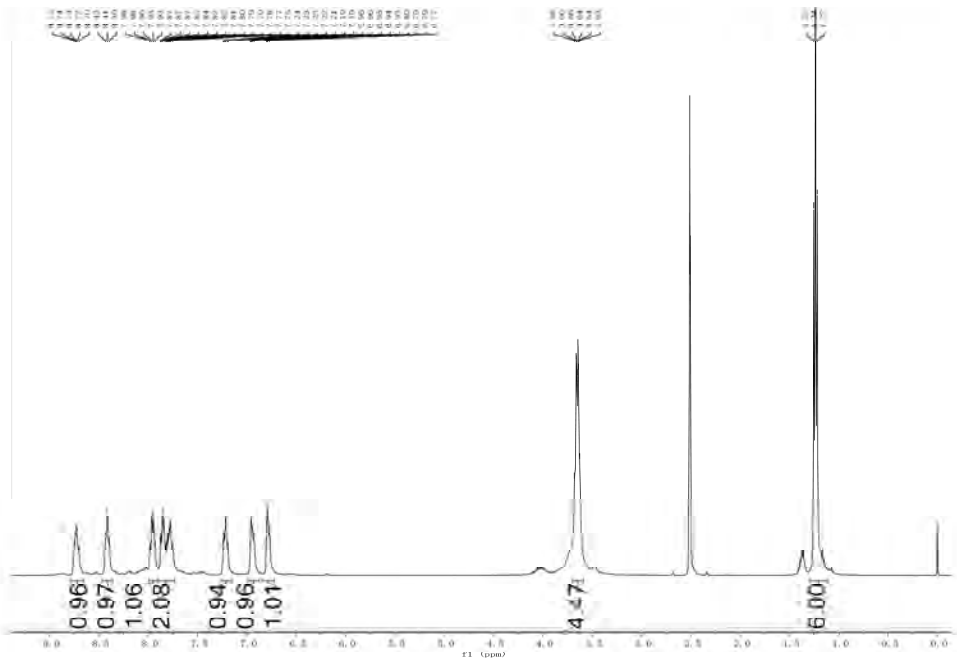

Figure S2. ^{1}H NMR spectra of NB-D

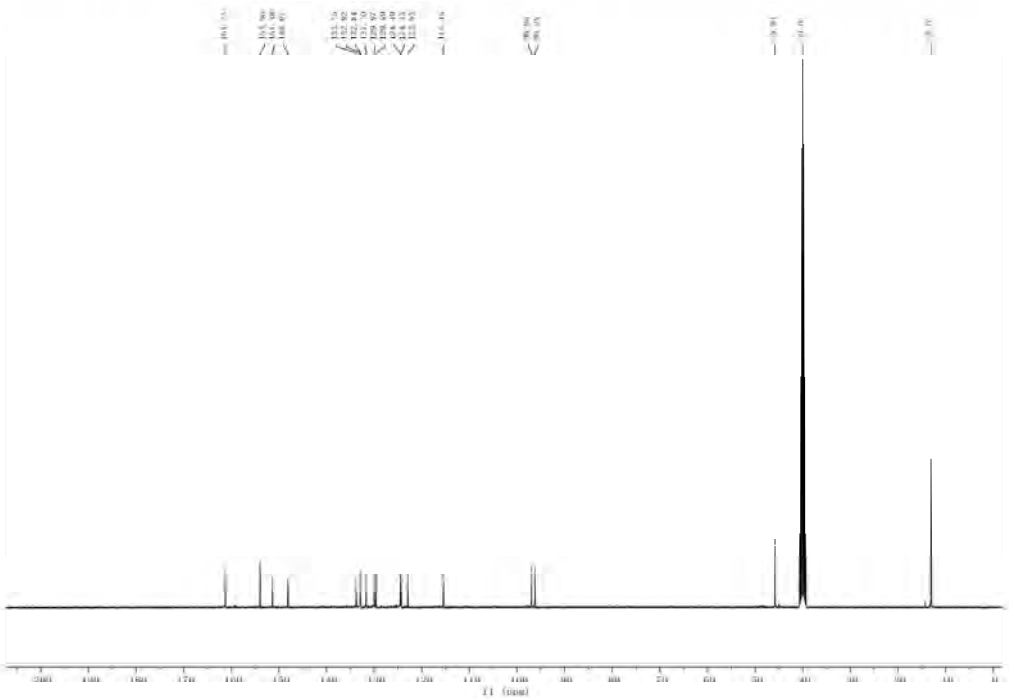

Figure S3. ^{13}C NMR spectra of NB-D

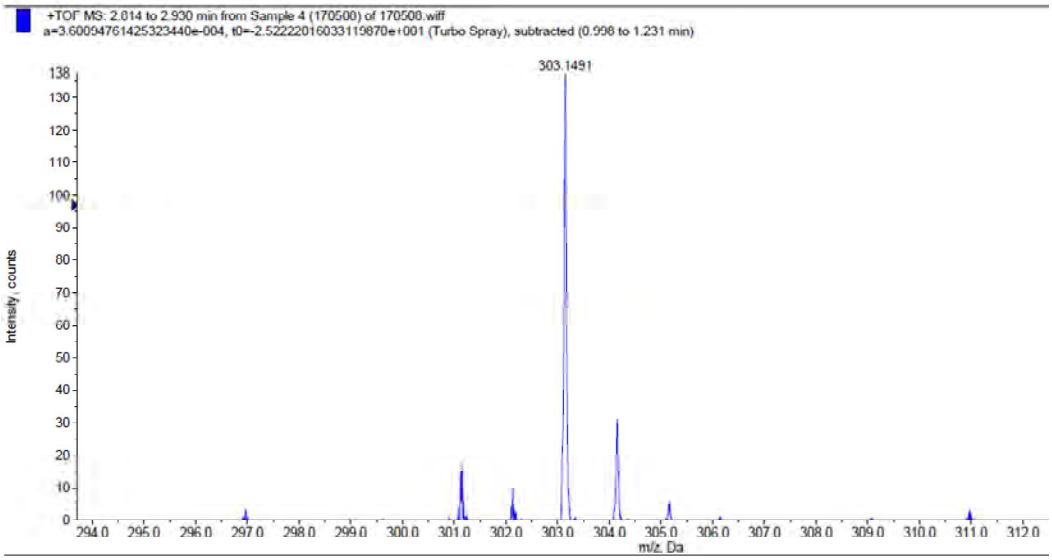

Figure S4. Mass spectra of NB-D.

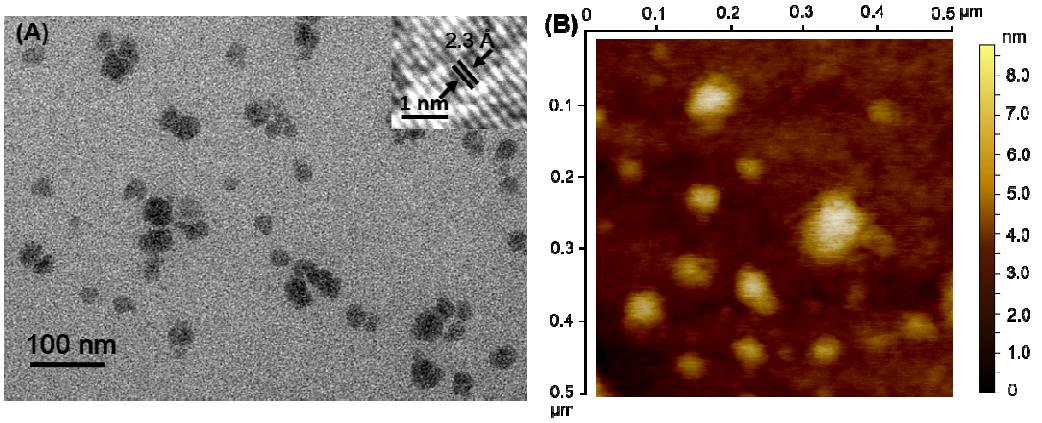

Figure S5. Characterization of BPs: (A) TEM and inset HR-TEM images; (B) AFM image of BPs

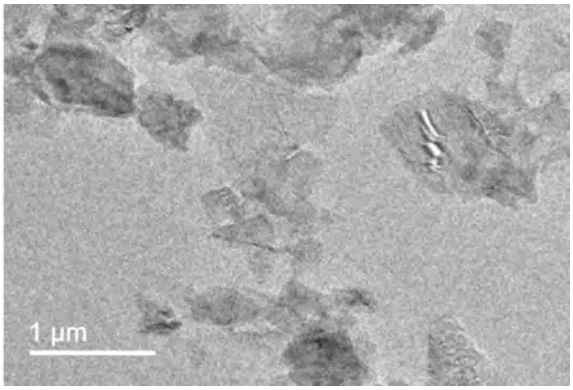

Figure S6. TEM image of micro-sized BPs synthesized by the liquid exfoliation method.

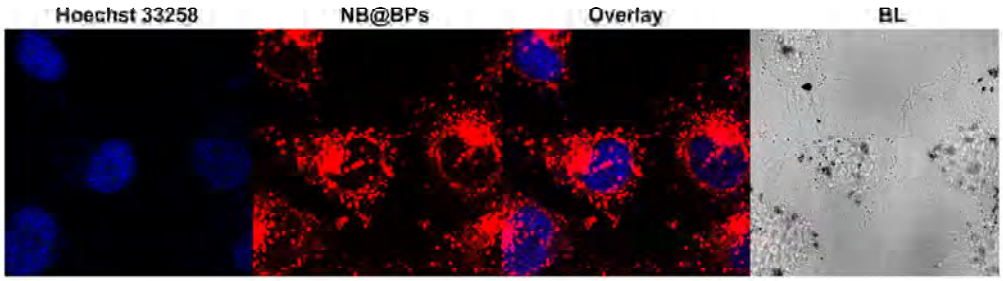

Figure S7. Confocal microscopic images of MCF-7 cells with 25 ppm NB@BPs for 3 h. Blue fluorescence refers to nuclei staiend by Hoechst 33528, and red fluorenscence refers to NB@NBs. BL refers to bright light.

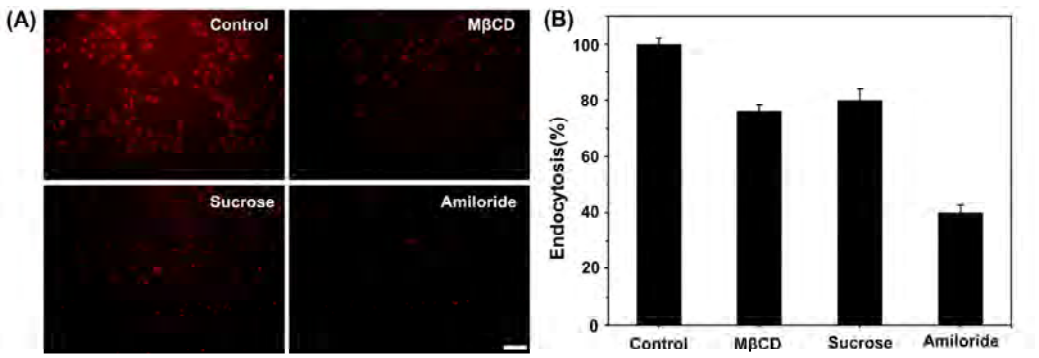

Figure S8. Inhibition of endocytosis with different inhibitors to evaluate mechanism of NB@BPs cellular uptaken by MCF-7 cells. (A) Fluorescence micrographs; (B)Intracellular fluorescence intensity of MCF-7 cells under different treatments: no treatment (control), MβCD (10 mM), sucrose (450 mM) and amiloride (2 mM). MCF-7 cells were treated for 2 h with each inhibitor, then the medium was replaced by fresh medium with 25 ppm NB@BPs for 2 h. To further quantify the intracellular fluorescence intensity, the cells were lysed with RIPA lysis buffer, and the intensity of fluorescence from NB@BPs was measured on a fluorescence spectrophotometer. The data are shown as mean ± SD (n=3). (Scale bar = 50 μm)

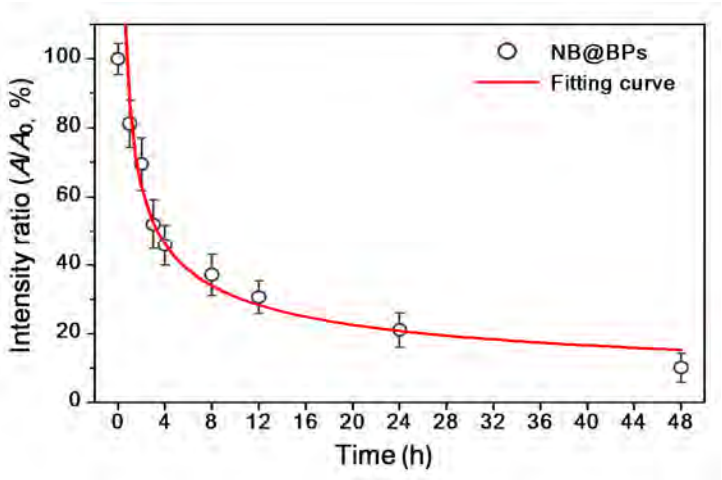

Figure S9. Fluorescence intensity ratios (A/A_0) in blood at different time points post-injection of the NB@BPs, where A and A_0 are the fluorescence intensities at time A and at 0 h post-injection (A_0).